and 10dB bandwidths were, respectively, 80 and 140nm. Out of the transmission bandwidth, the |TF| dramatically decreases from –10dB to the minimum accurately measurable value (–50dB) within ~40nm (i.e. the slope reaches 1dB/nm). The measured values of the transmission bandwidth are approximately two times narrower than the computed values. In accordance with theoretical predictions, this narrowing is attributed to the unexpected irregularities of the actual index profile. However, the bandwidth of the manufactured fibre remains large enough for many nonlinear applications. In spite of the noted discrepancy, the spatial filtering behaviour of the fibre around 1060nm is clearly pointed out. Further measurements are planned with newly manufactured fibres.

Conclusion: In this Letter, the modulus of the transfer function (|TF|) of a depressed-core-index photonic-bandgap (DCI-PBG) fibre has been studied both theoretically and experimentally. It has been shown that the theoretical 3dB bandwidth of 40cm of cladding fibre with seven high index layers, designed for transmission at 1060nm, is ~150nm. Experimental measurements with a 40cm piece of manufactured DCI-PBG fibre exhibit a 3dB bandwidth of 80nm around 1080nm. The slope of the |TF| reaches 1dB/nm out of the transmission bandwidth. The narrower measured bandwidth is due to imperfections in the actual profile. However, it remains large enough for nonlinear applications such as parametric amplification. Further measurements dealing with chromatic dispersion, which is supposed to exhibit zero dispersion at the central wavelength of the bandwidth, are currently being investigated.

F. Brechet, P. Leproux, P. Roy, J. Marcou and D. Pagnoux (*Institut de Recherche en Communications Optiques et Microondes, UMR CNRS 6615, 123 Avenue Albert Thomas, 87060 Limoges cedex, France*)

E-mail: brechet@ircom.unilim.fr

References

1 YEH, P., YARIV, A., and MAROM, E.: 'Theory of Bragg fiber', *J. Opt. Soc. Am.*, 1978, **68**, (9), pp. 1196–1201
2 MARCOU, J., and ROY, P.: 'Monomode photonic band gap fibers for dispersion shifting towards short wavelengths'. Proc. European Conf. Optical Communication, Nice, France, 1999
3 BRECHET, F., ROY, P., MARCOU, J., and PAGNOUX, D.: 'Singlemode propagation into depressed-core-index photonic-bandgap fibre designed for zero-dispersion propagation at short wavelengths', *Electron. Lett.*, 2000, **36**, (6), pp. 514–515

Hierarchical genetic image segmentation algorithm based on histogram dichotomy

Hanchuan Peng, Fuhui Long, Zheru Chi, David Dagan Feng and Wanchi Siu

A new hierarchical distributed genetic algorithm for image segmentation is proposed based on histogram dichotomy without an *a priori* number of image regions. Experimental results show that the proposed method outperforms the original distributed genetic algorithm.

Introduction: Image segmentation, one of the most important and difficult tasks in image/video processing, is the process by which an image is segmented into a group of non-overlapping homogeneous regions. Among various genetic image segmentation methods [1 – 3], the distributed genetic algorithm (DGA) [2, 3] has

been proposed as a simple but effective technique for parallel and unsupervised segmentation. Unfortunately, DGA needs the predefined image region number and often produces unpredictable poor results due to improper initialisation. To improve both segmentation quality and computational efficiency, in this Letter we propose a hierarchical distributed genetic algorithm (HDGA), which consists of two stages: quantisation and segmentation. Based on hierarchical histogram dichotomy, the stage of image quantisation utilises the statistical information of the image and provides a reasonable initialisation for the genetic algorithm. Based on the genetic algorithm, the image segmentation stage explores the spatial connectivity of the image and produces meaningful homogeneous regions.

Histogram dichotomy: In image quantisation, the image histogram is repeatedly dichotomised into hierarchical continuous intervals until every interval has a pixel-by-pixel mean square error (MSE) less than a given threshold T_σ. The histogram MSE on the grey level interval $[d, u]$ is defined as

$$\sigma^2_{[d,u]} = \sum_{k=d}^{u} P(k)(k - r_{[d,u]})^2 \Big/ \sum_{k=d}^{u} P(k) \qquad (1)$$

where d and u are lower and upper limits of the current histogram interval, the function $P(k)$ is the normalised greyscale histogram $(\Sigma_k P(k) = 1)$, and r is the quantised grey level of the histogram interval, as defined in eqn. 2:

$$r_{[d,u]} = \sum_{k=d}^{u} P(k)k \Big/ \sum_{k=d}^{u} P(k) \qquad (2)$$

When the MSE of a histogram interval is larger than T_σ, this interval will be split into two subintervals, the MSE sum of which is minimised, i.e. the interval division point $c_{[d,u]}$ is chosen as

$$c_{[d,u]} = \arg\min\left\{ \sigma^2_{[d,c]} + \sigma^2_{[c+1,u]} \right\} \qquad (3)$$

Using the above method, a hierarchical quantisation tree of histogram intervals is obtained. Each histogram interval corresponds to one or more image regions, which have the approximate homogeneity in the sense of the minimal MSE. It can be observed that the sum of interval MSEs in a higher level is always smaller than that in the lower level. This method is in accordance with the optimal image quantisation method [4]; however, the quantisation tree enables the quantisation quality to be controlled, without an *a priori* number of image regions.

Note that generally there are strong noises in the quantisation image, especially for slowly varying areas of grey levels. In addition, the spatial connectivity of an image is not considered in quantisation. Hence we present the following genetic paradigm.

HDGA: As with the DGA, in HDGA the genetic population is composed of all pixel chromosomes.' However, in contrast to the DGA, where a chromosome has three parts (pixel grey level, label, and fitness), in HDGA a pixel chromosome $l_{m,n}$ for the image pixel (m, n) consists of only two parts: label $b_{m,n}$ and fitness $f_{m,n}$. The chromosome label is defined as the pixel quantisation level and initialised using the histogram dichotomy results. The chromosome fitness is defined as

$$f_{m,n} = -\left| b_{m,n} - \frac{1}{H_{m,n} - 1} \sum_{p,q \in \Omega_{m,n}, p \neq m, q \neq n} b_{p,q} \right|$$
$$(1 \le m \le M, 1 \le n \le N) \qquad (4)$$

where $\Omega_{m,n}$ is a neighbouring area of the pixel (m, n), $H_{m,n}$ is the total number of pixels in $\Omega_{m,n}$, and M and N are the image width and height, separately. This new fitness function can better utilise the spatial connectivity in the input image than the original fitness function of the DGA [2, 3].

Three revised genetic operations are used in HDGA:
(i) Selection: select the $l_{p,q}$ with the greatest fitness $f_{p,q}$ in $\Omega_{m,n}$ to replace $l_{m,n}$.
(ii) Crossover: randomly cross over $l_{m,n}$ and $l_{p,q}$, which has the greatest fitness $f_{p,q}$ in $\Omega_{m,n}$, and 'binarise' the result to be one of these two parents.

(iii) Mutation: randomly select one $l_{p,q}$ in $\Omega_{m,n}$ to replace the current chromosome $l_{m,n}$. A small mutation rate r_m is defined.

The whole HDGA process is organised using the above three genetic operations. In every generation, after all the genetic operations, the total number of chromosomes that do not change labels is counted and the unchanged rate r_u is calculated. If r_u is larger than a preset threshold T_u in two continuous generations, then the HDGA stops. Otherwise a new generation begins.
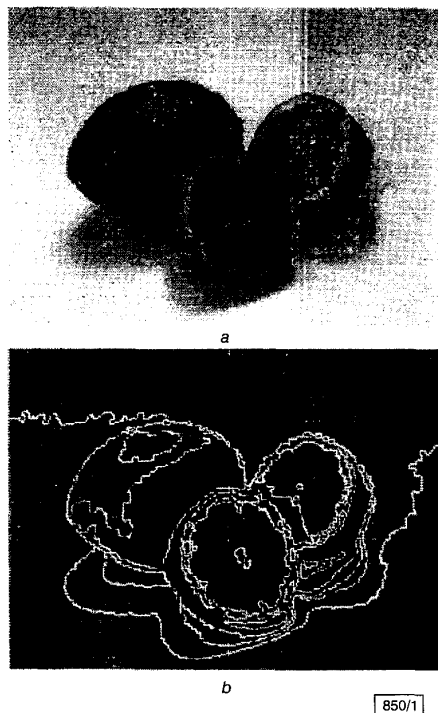

Fig. 1 *Segmentation result of HDGA*

a Input image
b Edges of HDGA segmentation regions

Experimental results: A computer simulation was carried out on a database of 1000 images, which belonged to five categories: children, men, frame pictures, business goods, fruit and vegetables. In each category there were 200 true-colour (24-bit) 320 × 240 images. In our experiments each image was converted to a 256 grey level (8-bit) image. For the following results, the HDGA parameters were $T_\sigma = 77$, $T_u = 0.9$, $\Omega_{m,n} = 3 \times 3$ neighbourhood of pixel (m, n), $r_m = 0.001$. For comparison, DGA's parameters were set the same as those of HDGA, or carefully adjusted to the optimum according to [2].

The HDGA and DGA were compared for every image in the database. For example, for the input image in Fig. 1*a*, the HDGA histogram dichotomy produces a quantisation tree, where the histogram division point list is '7, 17, 39, 58, 81, 107, 120, 146, 159, 181, 210, 227'. In comparison, the histogram division point list of the DGA is '19, 38, 58, 78, 97, 117, 137, 157, 176, 196, 216, 235' because the DGA uses uniform quantisation [2]. The image region edges after HDGA segmentation are shown in Fig. 1*b*. Note that HDGA effectively makes use of both the image statistical information and spatial connectivity. On the contrary, image regions produced by the DGA (not shown here for reasons of space) are usually more incoherent and less significant.

In Fig. 2 the convergence of the HDGA and DGA is compared (for Fig. 1*a*). Obviously the HDGA converges much faster than the DGA. For other images, the HDGA typically needs only ~ about ive generations while the DGA needs ~30–50 generations. Two possible causes are the better initialisation and improved genetic algorithm. In addition, even in one generation, the actual computation required by the HDGA is much less than that required by the DGA, due to the simplified chromosome structure and refined genetic operations. Furthermore, in our experiments (Matlab codes running on a PIII 550 PC machine), the histogram

dichotomy usually costs ~0.5s, whereas the genetic segmentation often costs more than 150s. Thus histogram dichotomy is computationally efficient in the HDGA.
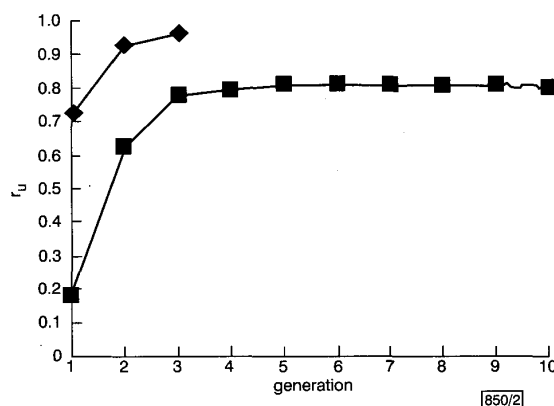

Fig. 2 *Convergence of HDGA and DGA*

◆ HDGA
■ DGA

Table 1: Indexes of image segmentation and removing quantisation noise

Category	Average S_σ[HDGA]	Average S_σ[DGA]	S_σ[HDGA]/ S_σ[DGA]	r_r[HDGA]
			%	%
Children	319.6175	401.8327	79.54	42–55
Men	310.6658	411.1724	75.56	35–47
Frame pictures	284.7555	402.6727	70.72	38–50
Business goods	280.6534	369.0727	76.04	44–52
Fruit and vegetables	310.6988	404.2918	76.85	28–42

We quantitatively evaluated the segmentation process by examining the homogeneity of the final image segmentation regions. The sum of the MSEs over all regions in a segmented image, i.e. $S_\sigma = \Sigma\sigma^2$, was calculated as the index. Better segmentation should produce smaller S_σ. The second and third columns of Table 1 show the average results for the HDGA and DGA for the five image categories. Clearly, the image regions produced by the HDGA have better internal coherence than those produced by the DGA. Actually, S_σ[HDGA] is 20–30% less than S_σ[DGA], as indicated by the fourth column of Table 1. We also examined the role of the genetic algorithm in removing image quantisation noise. Owing to the difficulty in counting small image regions, an index of the image region edge pixel reduction rate, r_r, was used as an approximation. The fifth column of Table 1 shows that the total number of image region edge pixels decreases significantly after the HDGA. The positive results of r_r are mainly due to the disappearance of small noisy regions.

Conclusion: The proposed HDGA can take advantage of statistical information and spatial information to segment an image. Experimental results show that the HDGA outperforms the DGA in both computational efficiency and segmentation quality.

Hanchuan Peng, Fuhui Long, Zheru Chi, David Dagan Feng and Wanchi Siu (*Center for Multimedia Signal Processing, Department of Electronic and Information Engineering, The Hong Kong Polytechnic University, Hung Hom, Kowloon, Hong Kong*)

E-mail: phc@eie.polyu.edu.hk

Hanchuan Peng: Also with the Department of Biomedical Engineering, Southeast University, Nanjing 210096, People's Republic of China

Hanchuan Peng: Corresponding author

References

1 BHANDARKAR, S.M., and ZHANG, H.: 'Image segmentation using evolutionary computation', *IEEE Trans. Evol. Comput.*, 1999, **3**, (1), pp. 1–21

2 ANDREY, P., and TARROUX, P.: 'Unsupervised image segmentation using a distributed genetic algorithm', *Patt. Recog.*, 1994, **27**, (5), pp. 659–673

3 LONG, F., ZHENG, N., and ZHANG, X.: 'A new image segmentation method based on genetic algorithm of multilayer perceptron', *Control Theory Appl.*, 1998, **15**, (2), pp. 232–236

4 SCHEUNDERS, P.: 'A genetic Lloyd-Max image quantization algorithm', *Patt. Recog. Lett.*, 1996, **17**, pp. 547–556

Optical image encryption using interferometry-based phase masks

Jong-Yun Kim, Se-Joon Park, Cheol-Su Kim,
Jang-Geun Bae and Soo-Joong Kim

A new and simple image encryption scheme and optical decoding technique are presented based on the principle of interference. An original image is encoded into two phase-valued images. The interference image between the two images produces a binary image, which has a two-level intensity value. The performance of the proposed technique is evaluated using computer simulations and optical experiments.

Introduction: Information fraud is a serious problem facing banks, businesses, and consumers. There is therefore a real need for a fast and reliable system for the identification of individuals, and verification of cards and IDs. Certain optical processing and pattern recognition applications have already been proposed for the security verification of credit cards, passports, and other forms of biometric image identification [1 – 4]. This Letter presents a new and simple optical security verification technique based on the principle of interference. A randomly generated reference image and encrypted image are made of the original image in the encoding process using computer processing and lithography. The encoded image is then decrypted by interfering the two-phase masks in an interferometer.

Interference between two waves: Let the two plane waves propagating in the z-direction with the same frequency ω, wavelength λ, amplitude E_0, and polarisation be

$$E_1(z,t) = E_0 \cos(kz - \omega t)$$
$$E_2(z,t) = E_0 \cos(kz - \omega t + \delta)' \quad (1)$$

where δ is the phase difference between the two plane waves, and k is the propagation constant. The intensity of the superposition wave of the two waves at an instantaneous time can be written as

$$I = \langle E_1 + E_2 \rangle^2$$
$$= \langle E_1 \rangle^2 + \langle E_2 \rangle^2 + 2\langle E_1 E_2 \rangle$$
$$= 2E_0^2(1 + \cos \delta) \quad (2)$$

If the phase difference between E_1 and E_2 is an even or odd multiple of π, the intensity of the interference pattern assumes a maximum or minimum value. Accordingly, since the interference pattern has a two-level intensity value, it can be changed to a binary image after thresholding. As a result, a certain intensity distribution can be considered as a combination of a pair of phase distributions. If one phase distribution out of the pair is known, the other can be easily determined from the interference intensity distribution. Finally, the binary intensity image can be represented by interfering the two phase images. This idea can be applied to the new encryption of the binary image.

Image encryption based on interferometry: Consider the case where two phase-only images are placed in each arm of a Mach-Zehnder interferometer, respectively, and every pixel in the two images has a phase value of '0' or 'π'. If two pixels with the same phase value interfere with each other, the corresponding intensity value will be

the maximum of '1', and pixels with a different phase value will result in the minimum value of '0'. Therefore, the binary intensity image can be represented by placing the phase images, which consist of phase values of '0' and 'π', in the two positions where the optical path difference between the two split waves is an integer multiple of 2π. The two images are referred to as a reference image and encoded image. The process of generating the two phase images is as follows. First, the binary random phase image for the reference image is generated with values of '0' and 'π'.

Table 1: Image encryption rule

Original image (intensity)	Reference image (phase)	Encrypted image (phase)
0	0	π
	π	0
1	0	0
	π	π

Next, the encrypted image is produced based on the proposed encryption rule in Table 1. For example, suppose the intensity value of a pixel in the original image is '0', and the phase value of a corresponding pixel in the reference image is '0'. The phase value of the pixel in the encoded image, which interferes with the pixel in the reference image, should be 'π'. If the phase value in the reference image is 'π', the phase value in the encoded image should be '0'. This rule is then applied to all the other pixels, thereby generating the encrypted image. For example, let the character 'T' be the original image to be encrypted, as shown in Fig. 1a. The reference image, which is a random binary phase image, is shown in Fig. 1b and the image shown in Fig. 1c is the encrypted image of the original image in Fig. 1a.
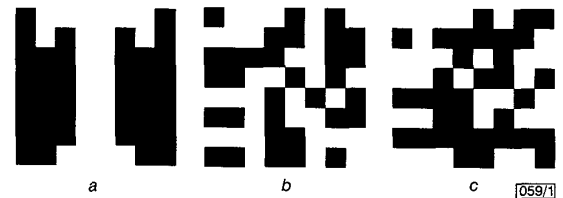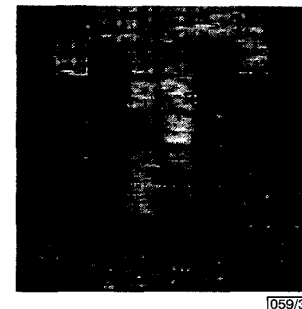

Fig. 1 *Generation of encrypted image*

a Original image
b Reference image
c Encrypted image
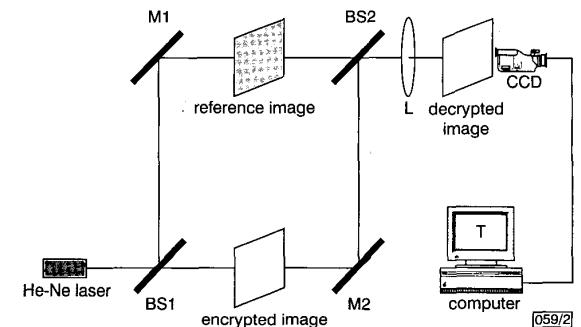
Fig. 2 *Optical security system for image decryption*

Fig. 3 *Optically decrypted image*